EXPERIMENTAL STUDY ON WHISTLING TONE FORMATION IN ROCKET NOZZLE THROATS

Ralf Stark, Carla Rieping, Stephan General, Jan van Schyndel, Clara Morris
German Aerospace Center, D-74239 Lampoldshausen, Germany

KEYWORDS: Rocket Nozzle, Throat, Tone Formation, Whistling

The formation of whistling tones within the nozzle throat is suspected to be a source of rocket nozzle exhaust jet noise. To study this tone formation, a set of orifice plates with varying geometries and diameters was tested, and compared with several convergent-divergent nozzles. The results confirmed the presence of distinct tones, formed in the orifice plates and the nozzle throats, which clearly correlated with the related diameter, respectively. The orifice plates demonstrated to serve as effective nozzle throat surrogates in respect to acoustic properties. In addition, a way was found to suppress the formation of whistling tones.

1. INTRODUCTION

Rocket engines generate extremely high noise levels that have a significant impact on the structures of the launch pad, the rocket itself and the payload. The generation of noise can, in part, be attributed to the rocket nozzle exhaust jet. This so called jet noise (JN) consists of several mechanisms that originate within the exhaust jet itself or arise from its interaction with the surrounding environment or the nozzle structure. Insights into the noise-producing mechanisms can be useful to reduce the overall acoustical load. The main components of JN are turbulent mixing noise and shock-associated noise. Both exhibit characteristics that are partly direction-dependent.

1.1 Turbulent mixing noise

Turbulent mixing noise (TMN) has been identified as the predominant source of noise generation in shock-free jets [1] and is significantly influenced by jet Mach number M_j and temperature [2]. For subsonic flow, the sound pressure level (SPL) attributed to TMN increases with rising temperature [1], whereas in supersonic flow the noise level decreases [3].

TMN arises from both small-scale and large-scale turbulence structures. The small-scale turbulence structures dominate the noise emission in lateral and upstream direction around the jet axis (70° to 130°), whereas the large-scale turbulence structures are primarily responsible for the downstream noise emission (<70°) [4, 5]. This directional dependence becomes more pronounced as the exit velocity increases.

Additionally, the generation of Mach waves can be attributed to the large-scale turbulence structures, which also contribute to the overall noise level [4]. Mach waves arise when the velocity at which the large-scale turbulence structures are transported by the flow exceeds the local speed of sound. The resulting noise is emitted within the related Mach cone that lies around the jet axis; its angle μ depends on the jet Mach number M_j.

1.2 Shock-associated noise

Shock-associated noise (SAN) arises from the interaction of downstream travelling turbulence and quasi-static shocks in supersonic exhaust jets [1, 6]. The dominant frequencies of SAN are higher than those of TMN, which simplifies their differentiation when examining the frequency spectrum [7]. The generated sound waves can propagate upstream to the nozzle lip, excite it, and amplify the shear layer instabilities [7]. This leads to a feedback mechanism and produces a clear, discrete tone known as a screech.

If no feedback mechanism is present, so-called Broadband-SAN (BB) dominates. Its spectrum consists of a main frequency, surrounded by frequencies of similar but slightly lower amplitude. The frequency spectrum additionally displays a number of peaks, the order of which is related to the spacing of shock-cells in the free jet [6].

BB exhibits a high directional dependence and can be observed particularly clearly at higher angles (upstream of the nozzle exit). With increasing observation angle, the main frequency amplitude increases and BB bandwidth becomes narrower [6]. In downstream direction, BB is often masked by the noise of the Mach waves.

1.3 Transonic resonance

Another mechanism contributing to noise generation is transonic resonance (TR). It is a nozzle-internal phenomenon that occurs when the flow separates inside the divergent section of the nozzle. Like screech, it is a feedback phenomenon [8], which begins with a disturbance of the boundary layer in the nozzle throat that propagates downstream towards the unstable separation. In the separation region it induces small vortices, which grow in the downstream shear layer. When these shear layer vortices leave the nozzle, they can excite the nozzle structure, leading to and enforcing the feedback of the disturbances in the throat. In contrast to screech, TR exhibits a staging behaviour between resonance modes that depends on the acoustic conditions in the separated nozzle section [8, 9].

The period in which TR can occur begins when the nozzle starts choking ($M_\mathrm{t} \geq 1$) and ends as soon as the separation zone reaches the nozzle exit. It has been shown experimentally that the TR amplitude is strongly influenced by the throat's surface structure [8, 9]. The feedback is prevented when the coupling with the throat boundary layer is disrupted [8–10]. The noise intensity and frequencies generated by TR depend on the Mach number of the separated jet M_{j}, the nozzle's angle of divergence [8] and the exhaust jet temperature.

1.4 Characteristic tones

In addition to the JN, most nozzles produce a specific, characteristic tone [10–13]; where the author's past experience collected while testing different prototypes has shown that a larger nozzle produced a deeper tone. During nozzle operation, with increasing total pressure, this characteristic tone shifts to lower frequencies (Croissant shape, [11]).

The literature suggests that these characteristic tones originate in the throat of the rocket nozzle [9]. But, studying this presumed correlation with several nozzles experimentally is not only time-consuming concerning the design, construction and manufacturing process, but also expensive. However, the literature also contains limited studies on the formation of whistling tones from orifice plates, which showed that the generated tones are related to the orifice diameter [14].
It was therefore decided to study several (quick and inexpensive to produce and test) orifice plates experimentally that are not only intended to represent the acoustic properties as a generic nozzle throats, but demonstrably do so.
For this purpose, a set of nine plates was manufactured, which differ in orifice diameter and the related inlet and outlet geometries. To prove that the orifice plates represent nozzle throats, several already available nozzles were also studied for comparison under the same test conditions.

2. TEST SETUP

The experimental study was conducted at DLR's cold flow subscale test facility P6.2 in Lampoldshausen. The facility offers dry gaseous nitrogen as the working fluid, which was stored outside at ambient temperature in 20 MPa high-pressure vessels. A supply system, consisting of an automatic valve, a particle filter, a dome pressure reducer, a regulation valve, and a mass flow meter, connected the storage vessels with a settling chamber that was mounted on a horizontal thrust frame (Fig. 1). The settling chamber was equipped with a set of grids and honeycombs to homogenise the flow. The setup featured a maximum total pressure upstream the test specimens of p_0 = 6 MPa, with a maximum mass flow rate of 4.2 kg/s.

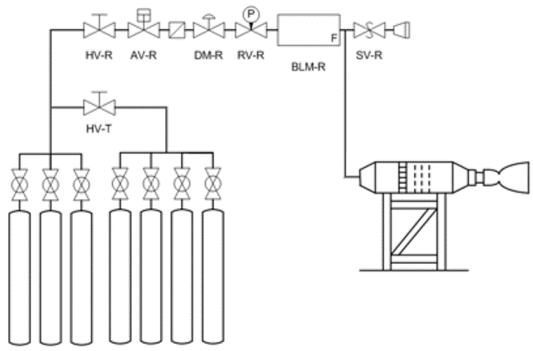

Figure 1: P6.2 supply system.

2.1 Test specimen

To study the formation of whistling tones in generic rocket nozzle throats, three sets of orifice plates were manufactured. Each of these sets consists of three plates that share the same throat diameter but differ in throat geometry, and hence, the boundary layer flow path length (see Fig. 2).

The related in- and outlet radii were scaled with the throat diameter, with the inlet radius being R_{WTU} = 0.5 D_{t} and the outlet radius R_{WTD} = 0.25 D_{t} (see Tab. 1). These geometric relations correlated with the standard throat geometry of nozzles that have already been tested at DLR in the past.

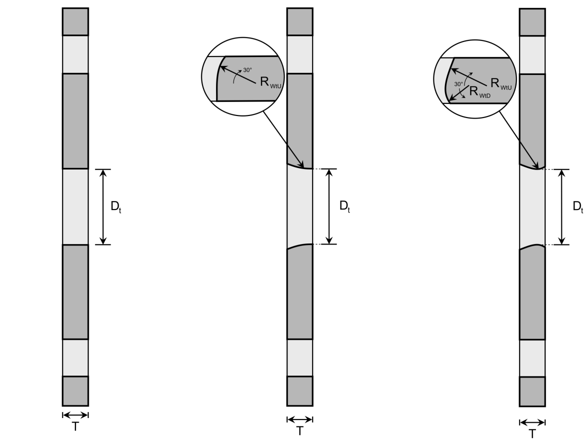

B20-0: no radii *B20-1: inlet radius* *B20-2: in- & outlet radii*

Figure 2: Throat geometries.

The name of each plate is composed of *B* (German term for orifice plate *Blende*), followed by its throat diameter, and the number of throat radii. For example, B20-1 means a diameter of 20 mm with an inlet radius.

All plates featured a throat diameter to plate thickness ratio of D_{t}/T = 2.66. Fig. 3 gives an impression of B12-1 mounted on the test rig.

Table 1: Overview of plate geometries.

Plate	Diameter D_t mm	Height T mm	Inlet R_{WTU} mm	Outlet R_{WTD} mm
B12-0	12	4.5	-	-
B12-1	12	4.5	6	-
B12-2	12	4.5	6	3
B16-0	16	6	-	-
B16-1	16	6	8	-
B16-2	16	6	8	4
B20-0	20	7.5	-	-
B20-1	20	7.5	10	-
B20-2	20	7.5	10	5

2.2 Pressure and temperature measurements

The total pressure and the total temperature upstream of the test specimens was measured in the settling chamber, using a BM-350 type Intersonde pressure transducer and a standard PT1000 temperature sensor, with acquisition rates of 1 kHz and 0.1 kHz, respectively. An additional piezoresistive XT-154-190M type Kulite pressure transducer was mounted in a cross section upstream the test specimen (see Fig. 3). It was connected to the flow via perpendicular 0.5 mm orifice to enable 65.5 kHz high-frequency measurements. The aim was to cross-check the impact of possible supply system eigenfrequencies on whistling tone formation.

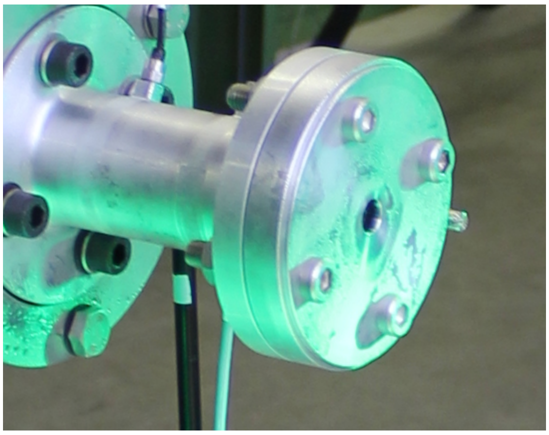

Figure 3: Specimen B12-1 mounted on test rig.

2.3 Acoustic measurements

For the acoustic measurements two different types of microphones were used. Six ½-inch 4966-H-041 type Brüel&Kjær microphones were placed along an arc above the specimens, which was centred to the middle of the specimen (Fig. 4). These microphones were positioned from 30° to 130°, in steps of 20°. During the course of the test campaign, the microphone at 30° was moved to 40°, as it was too close to the flow and reached the limit of its range.

Two ¼-inch 4941-A-011 type Brüel&Kjær microphones were initially attached to the arc at 80° and 100°. But,

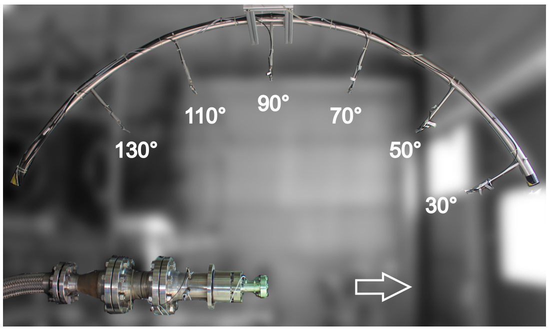

Figure 4: Far field microphones on arc.

in the course of the test campaign they were placed directly near the plates as their higher operating range of up to 184 dB enabled the recording of the characteristic tones directly near their source (Fig. 5, left).

All microphones were connected to LAN-XI 3050 type Brüel&Kjær modules, arranged in a mobile LAN-XI frame. Their signals were scanned with a rate of 65.5 kHz, and digital filters of 25 kHz were applied.

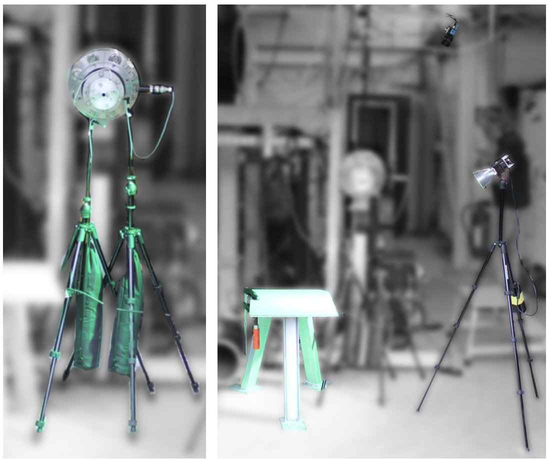

Figure 5: Near field microphones (left) and BOS setup (right).

2.4 Flow visualisation

The exhaust jet flow was visualised using the Background Oriented Schlieren (BOS) technique. BOS has the advantage of a much simpler experimental setup compared to traditional Schlieren imaging methods, where large lenses or parabolic mirrors have to be precisely aligned. The BOS method only required a structured background, a (preferably monochromatic) light source for illumination and a camera recording the background (Fig. 5, right). The recorded images were evaluated with the in-house DLR software BOSVIS [15]. This software uses an optical flow algorithm [16] to determine the displacement of each individual pixel in the recorded images, which is caused by gradients in the refractive index of the propagating medium. The results were processed images, or combined as a video, in which the structures of the exhaust jet flow were clearly visible.

2.5 Test sequence

All specimens were tested with a standardised test sequence in which an up/down-ramping was repeated five times.

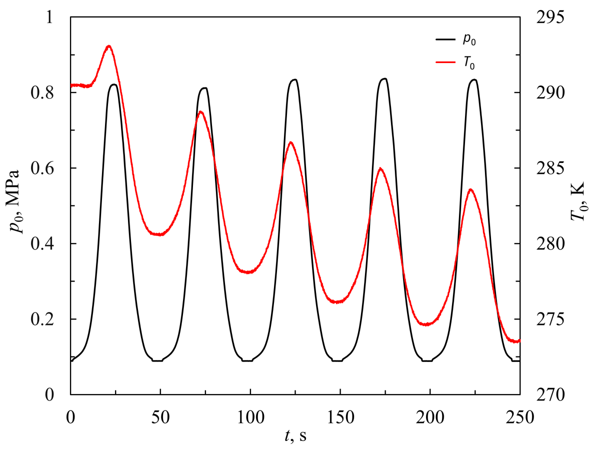

Figure 6: Test sequence with five repetitions (B12-2).

Fig. 6 illustrates the related total pressure profile. Steep total pressure increases were followed by short-time pressure plateaus and completed by in turn steep decreases. Due to the quasi adiabatic expansion within the storage vessels over test time, the related total temperature profile displayed an overall decreasing trend, which, however, has a virtually negligible effect on the speed of sound.

2.6 Reference nozzles

To demonstrate the transferability of the plate results, four nozzles, which had already been tested in the past, were studied experimentally again, using the same test setup and test sequence.
As plate B20-2, all nozzles featured the standard DLR throat geometry with a diameter of 20 mm, and the related in- and outlet radii. The nozzles differed in terms of their divergent length, i.e. their area ratio (ϵ = 2.86, 14.0 or 30.0) and the design of the nozzle throat (one-piece or in two parts). The specimen DLR-Sub featured only a subsonic inlet. Tab. 2 summarises their features.

Table 2: Tested nozzles.

Nozzle	ϵ	Throat	Ref.
TIC-2.86	2.86	one-piece	[17]
TIC-14	14.0	two parts	[18]
TICTOP B1	30.0	one-piece	[13, 19–22]
DLR-Sub	1.0	inlet only	-

3. RESULTS AND DISCUSSION

The acoustic test data of the plates, provided as pressure fluctuations, were processed using an in-house software. Calculating the RMS values and deriving the sound pressure level (SPL) firstly enabled the mapping of the spatial distribution of the noise emission.

The resulting spatial representations displayed no overall directional dependencies (Fig. 7), and hence excluded dominant TMN. The SPL increased only at an angle of 30°, which revealed the expected impact of Mach waves.

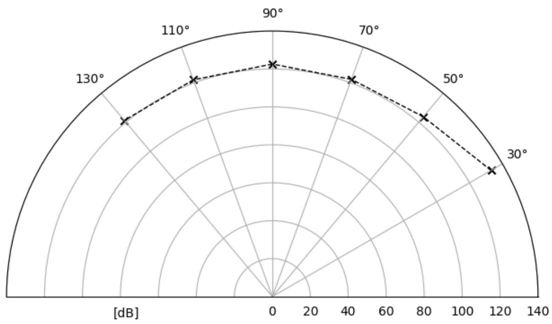

Figure 7: Spatial noise emission, B12-2.

Subsequently, multiple FFT calculations were carried out, which sequentially transformed small sections of the time-dependent pressure signals into the frequency domain and generated SPL levels from the results. Waterfall plots were derived, revealing the time evolution of the frequency spectra.

Fig. 8 gives a compilation of three directional waterfall plots. A broadband region is highlighted for each direction. With increasing observation angle (90° → 130°), the broadband region shifted towards lower frequencies. It was concluded that this illustrated the impact of Broadband-SAN (BB).

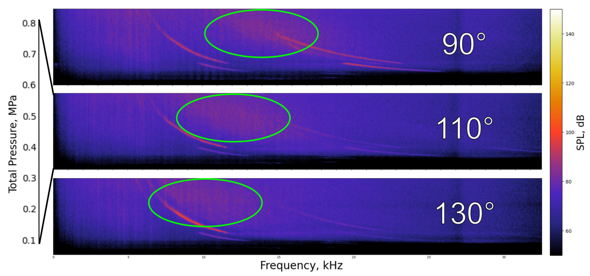

Figure 8: BB noise evolution, B12-2.

Given the presence of BB and the fact that in the overall analysis the detected distinct tones showed no directional dependence in terms of frequency and SPL, a screech phenomenon could be ruled out. Especially as both the plates and the nozzles featured thick-walled structures.

Fig. 9 displays the mentioned distinct tones more prominent using a spectrum progress of plate B20-2 (sequence phase: $t = 0 \rightarrow 50s$). Several tones were clearly visible. The frequencies changed with time, i.e. with total pressure. As the total pressure increased ($t = 5 \rightarrow 25s$), the frequency decreased, and vice versa ($t = 25 \rightarrow 45s$). In addition to the harmonic overtones, a brief frequency shift was noticeable.

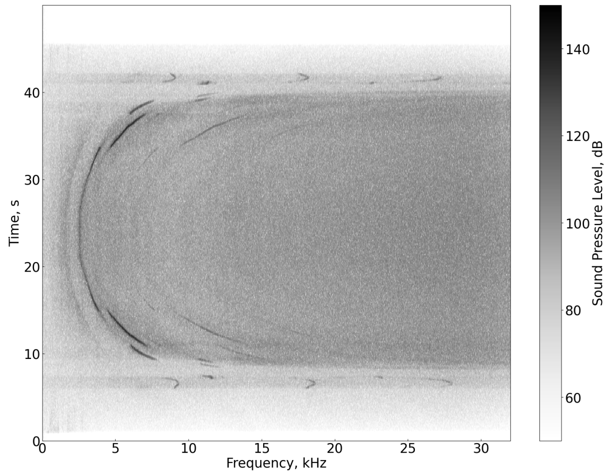

Figure 9: Whistling of B20-2.

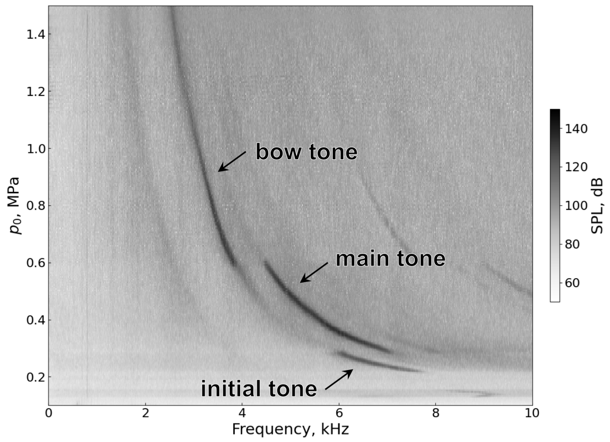

Figure 10: Definition of whistling tones, B20-2.

Fig. 10 illustrates the frequency shift with a zoom. Here, the test time was substituted by the total pressure. First, an initial tone appeared, which gave way to the main tone. Once the main tone ended, the bow tone started.

The initial tone appeared around a total pressure of $p_0 = 0.2\,\mathrm{MPa}$, where the plate started choking. If one takes into account the thickness T of the plate and thus the short flow path through the orifice, flow separation could be excluded, which rules out a transonic resonance as the cause of the tones.

Next, the tones appearing in the waterfall plots were approximated using polynomial fits, where for each specific microphone signal an up- and down-ramping polynomial was determined, representing all five repetitions. All of these specific polynomial fits were combined again to derive single trend lines representing the characteristic tones of the test specimen. Fig. 11 illustrates how the main tone trend line of plate B12-2 was generated from all the derived polynomial fits for a singular test run.

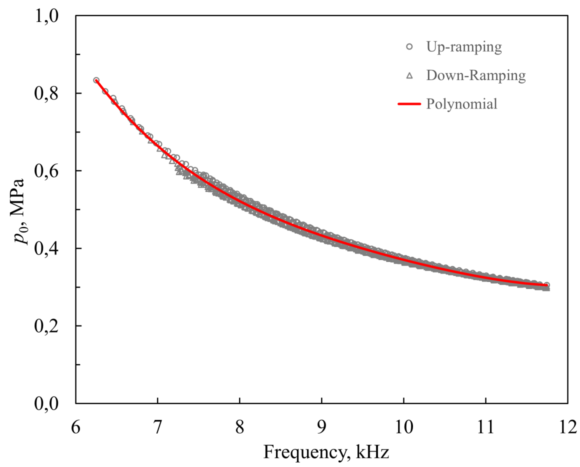

Figure 11: Example for polynomial-fitting, B12-2 main tone.

3.1 Initial tones

Fig. 12 summarises the derived initial tone trend lines for all plates. It is clear that a larger orifice diameter generated lower frequencies. The non-contoured plates B12-0, B16-0 and B20-0 exhibited a distinct feature. Their generated frequencies are shifted towards higher values and began later, i.e. at higher total pressures.

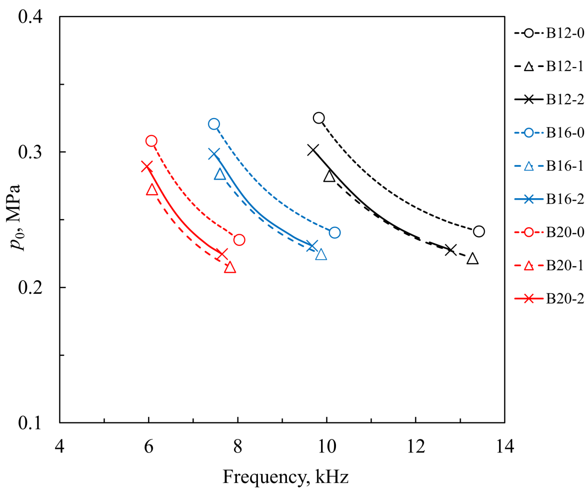

Figure 12: Initial tones of all plates.

The BOS images in Fig. 13 (both equal p_0/p_a) provided a possible explanation.
The left image (a) shows the supersonic exhaust jet of the contoured plate B20-2. An oblique separation shock could be seen, anchoring at the exit edge of the plate and initiating a typical shock train. In the lower half of the image, the shock system is highlighted in red.
The right image (b) reveals an additional internal shock that originated inside the non-contoured plate B20-0; marked as a blue line. This internal shock demonstrated that a supersonic flow was being deflected within plate B20-0. This was only possible if the inflow constricted and formed a 'virtual' convergent-divergent

nozzle throat. The diameter of the virtual throat was smaller than the geometric throat and therefore generated higher initial tones. The formation of a 'stable' virtual throat during the transient start-up of the plate was responsible for the delay in the pressure range.

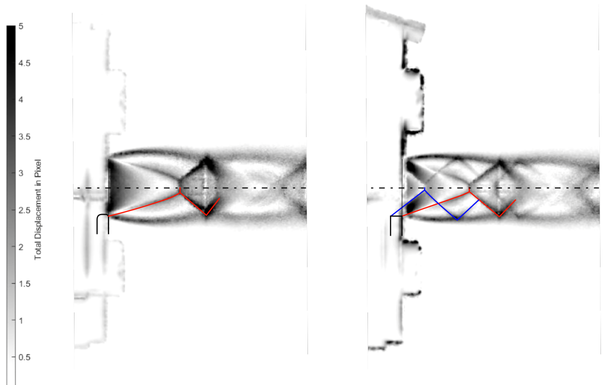

(a) B20-2 (b) B20-0

Figure 13: BOS visualisation of exhaust jets. Plate B20-2 with oblique re-compression shock marked in red (left), and plate B20-0 with additional internal re-attachment shock marked in blue (right).

3.2 Main tones

As the total pressure increased, the initial tone of all plates suddenly shifted to the higher frequency of the main tone. The trend lines for all main tones are shown in Fig. 14. At the start of the transition, the lines of the contoured plates are very close, whereas the frequencies of the non-contoured plates are higher. Except of plate B20-0, this effect diminishes as the total pressure increases. In addition, it could be concluded that the outlet radius had an influence on the generated frequencies. The inlet radius, on the other hand, determined the total pressure at which the transition to the main tones occurred.

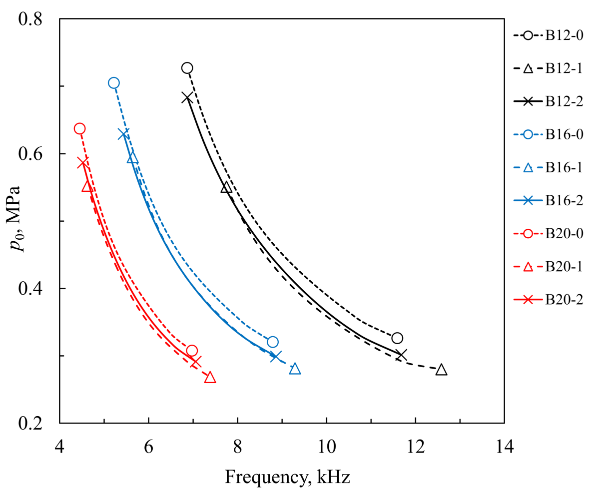

Figure 14: Main tones of all plates.

The re-transition back to the bow tone at higher pressures was often less clearly defined. It was gradual and sometimes masked by general jet noise. These ambiguities mostly occurred for the microphones mounted to the arc. The microphones positioned directly at the plates picked up the main tone across the widest range of total pressure.

3.3 Tone transition

Fig. 15 shows, for each orifice plate, the frequencies at which the respective initial tone ended (∇-symbols) and the subsequent main tone began (Δ-symbols), relative to the orifice diameter. Overall, it could be seen that the frequencies at which the initial tones ended are nearly identical for each orifice diameter. In contrast, the onset frequencies of the main tones differed; however they were always higher than the cut-off frequencies of the initial tones. It was striking that the contoured orifices with only an inlet radius (B12-1, B16-1, and B20-1) began with slightly higher main tone frequencies than the remaining orifice plates, whose onset frequencies were nearly identical. Overall, all frequency transitions showed similar magnitudes.

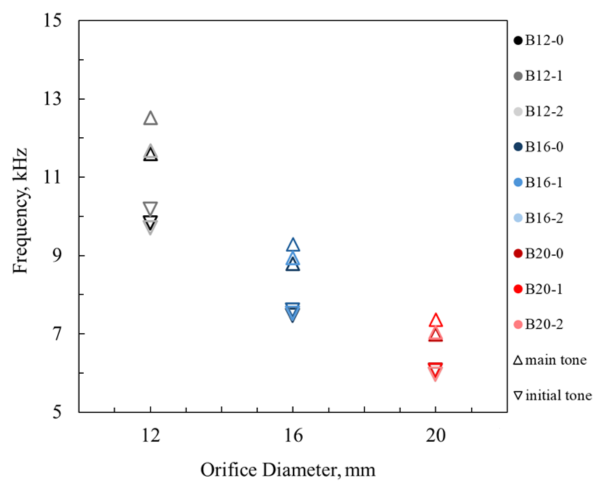

Figure 15: Frequency of tone transition.

Fig. 16 gives the transition from initial to main tone in relation to the total pressure. It could be seen that the orifice diameters had no impact on the transition pressures, but the transition pressures depended somewhat on the contour design. The plates with only an inlet radius (B12-1, B16-1 and B20-1) featured the lowest transition total pressures, followed by plates with inlet and outlet radii (B12-2, B16-2 and B20-2) and the plates without contours (B12-0, B16-0 and B20-0).

This result correlated with an effect that was already known: Experiments had shown that (within this total pressure range) temporary re-laminarisation of the boundary layer occured in the nozzle throat of comparable DLR TIC nozzles [23], which, in this case, lead to higher frequencies.

The normalised transition in frequency in Fig. 17 ($f=(f_{HT}-f_{IT})/f_{HT}$) illustrates the relationships more clearly. Regardless of the diameter, the frequency shift was highest for plates with an inlet radius (Δ-symbols), followed by plates with radii in both directions (×-

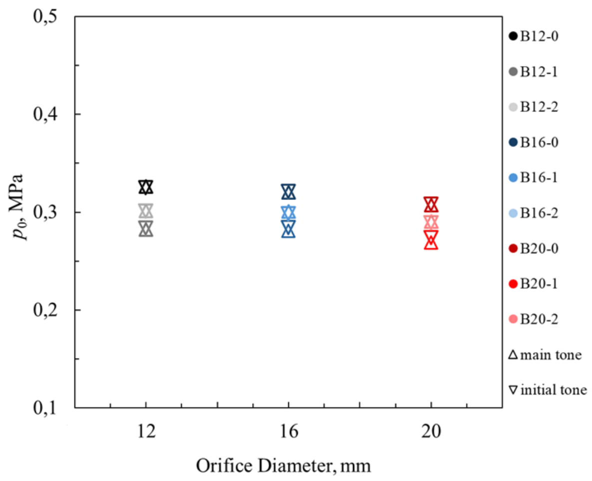

Figure 16: Pressure of tone transition.

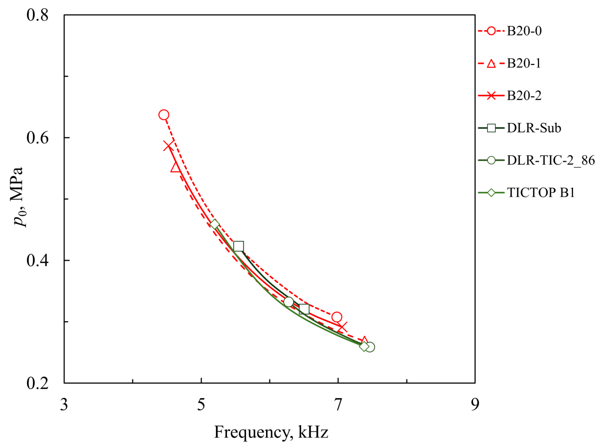

Figure 18: Acoustical behaviour of the compared nozzles.

symbols). The plates without radii (○-symbols) always exhibited the smallest percentage shift in frequency. The maximum frequency difference was five percentage points per set of plates, and on average, the magnitude of the frequency shift was approximately 16 % of the main tones' starting frequency.

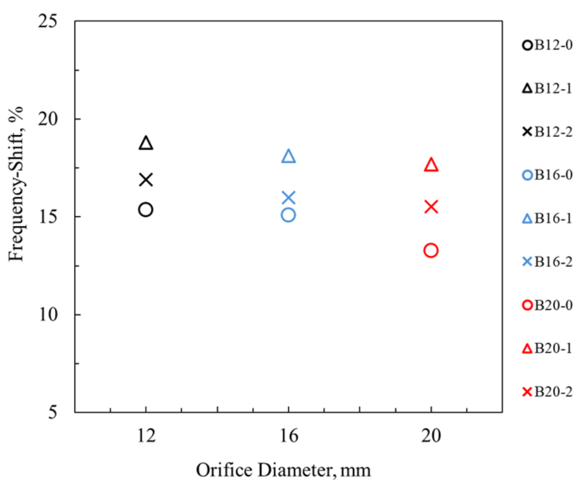

Figure 17: Normalised tone transition.

3.4 Comparison to nozzles

The nozzles tested for comparison produced main tones, but no initial tones. Consequently, no tone transition was exhibited. Fig. 18 compares the main tones of the nozzles with those of the plates with the same throat diameter of 20 mm.

A comparison of the trend lines showed that they were quite similar, but differ in their onset and end pressures. Contrary to the expectation that all nozzle tones would follow the established pattern of the plate B20-2 (with radii in both directions), the convergent-divergent nozzles showed greater correspondence with the trend of plate B20-1 that featured only an inlet radius. The main tones of the TICTOP B1 and the TIC-2.86 began at a similar total pressure compared to the plate B20-1, but ended earlier. This suggests that the location of the transonic region ($M_t \approx 1$) was crucial.

The main tone of the TIC-2.86 ceased after a total pressure increase of less than 0.1 MPa, whereas the main tone of the TICTOP B1 ceased after an increase of only 0.2 MPa.

The DLR-Sub, with its convergent inlet, differed from this behaviour. It began at a slightly higher total pressure than plate B20-0, and also ceased following a pressure increase of 0.1 MPa. Given the geometric similarity, it was expected that the trend line would resemble that of the plate B20-1.

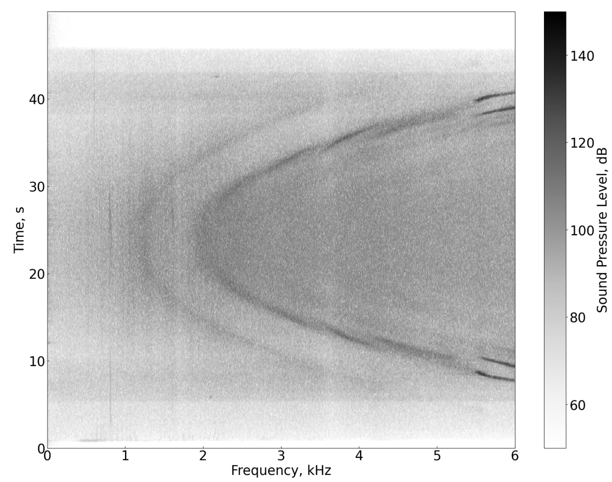

Figure 19: FFT-Time DLR-Sub Zoom.

In earlier experiments, the full-flowing TICTOP B1 revealed an characteristic tone of 1345 Hz [13]. This tone could not be reliably reproduced, as the nozzle was only tested under separated flow conditions. The DLR-Sub generated a tone that was lower than its bow tone and mirrored the bow tone course down to ~1.3 kHz (Fig. 19). The frequency of this tone was close to the characteristic tone of the TICTOP B1, suggesting that its characteristic tone also originated in its nozzle throat.

3.5 Suppression of tones

The TIC-14 nozzle, surprisingly, did not generate any characteristic tones. In comparison to all other nozzles and plates, this nozzle featured a two-part contour. Its convergent section was the DLR-Sub inlet and the divergent contour was attached to it, with the junction in the throat. TIC-2.86 produced only a main tone, whereas DLR-Sub also produced an initial tone. This suggested that the complete absence of a tone in the TIC-14 nozzle was attributable to the design differences between the nozzles.

The junction from the convergent to the divergent contour section (either a minor backward or a minor forward facing step) caused a disturbance in the boundary layer. Hence, it is hypothesised that distinct tones can only be generated when the throat boundary layer is undisturbed.

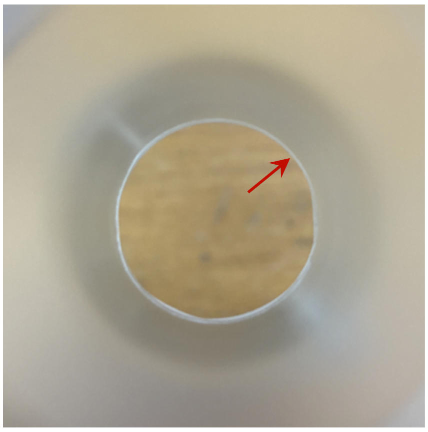

Figure 20: TICTOP B1 with circumferential throat protrusion.

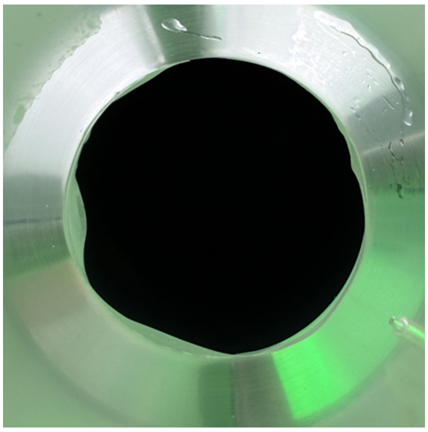

Figure 21: TICTOP B1 with iced throat.

To validate this hypothesis, the TICTOP B1 was tested again with a small protrusion applied in the throat, to disrupt the boundary layer (Fig. 20). The TICTOP B1 had previously produced a clear main tone. However, in this configuration, no tone was produced during the first ramp. Towards the end of the first ramp, it could be observed on the related BOS video that the protrusion was ejected from the nozzle. In the subsequent repetitions, the main tone then reappeared. This behaviour was reproduced in further test runs with the same result.
Further backing for this hypothesis was observed in one test where the tones cut out as the number of repetitions increased. This could be attributed to the rapid cooling of the nozzle and the formation of ice in the throat; causing a natural boundary layer disturbance (Fig. 21).
At a broader level, the authors' experimental experience has found that prototypes change their tonal behaviour after repeated test runs ($n \geq 10$). In these cases, the previously hydraulically smooth throat surface of the nozzle changes due to abrasion.

4. CONCLUSION

To study the formation of whistling tones in rocket nozzle throats nine generic orifice plates were studied experimentally, which differ in orifice diameter, orifice contour design and plate thickness. All plates generated whistling tones, where smaller orifice diameters produced higher tones (and vice versa). With increasing total pressures their tone frequencies decreased.

When the throats started choking an initial tone appeared that switched to a higher main tone. This transition was caused by a relaminarisation of the boundary layer.

The non-contoured plates featured virtual throats with an internal shock that could be proven by BOS videos of the exhaust jets. These virtual throats, with decreased orifice diameters, therefore generated higher tones.

The nozzles tested for comparison generated tones that were comparable with the plate set featuring the same orifice diameter.

A nozzle with a structural junction in its throat generated no whistling tones. This was hypothesised to have been caused by the resulting disturbance of the boundary layer. For hypothesis confirmation, a protrusion was placed in the throat of a one-piece nozzle, which resulted in tone suppression. In addition, a randomly appeared iced throat lead to the same result, confirming the hypothesis as well.

This is very much in line with the findings from past testing of prototypes. As the cumulative test duration increased, the throats suffered significant abrasive damage and the engines' characteristic tone amplitudes decreased or even vanished.

It has been shown that the characteristic tones of rocket nozzles originate in the nozzle throat. The generation of these whistling tones can be thoroughly studied using simple, representative orifice plates. The formation of these tones can be prevented by disturbing the boundary layer within the nozzle throat.

5. ACKNOWLEDGEMENTS

The authors would like to thank the test facility team H. Neumann, M. Erl, J. Reinhold, and P. Fuchs, which made the more than successful test campaign possible.

6. REFERENCES

1. Fischer, M. J., Lush, P. A., and Harper Bourne, M. (1973). Jet Noise. *Journal of Sound and Vibration* 283, pp. 563–585.

2. McInerny, S. (1990). Rocket noise - A review. In Proc. 13th Aeroacoustics Conference, American Institute of Aeronautics and Astronautics, Tallahassee, USA.

3. Tanna, H. K. (1977). An experimental study of jet noise part I: Turbulent mixing noise. *Journal of Sound and Vibration* 503, pp. 405–428.

4. Tam, C. K. W. (2009). Mach Wave Radiation from High-Speed Jets. *AIAA Journal* 4710, pp. 2440–2450.

5. Costa Ruiz, E., Stark, R., Génin, C., and Oschwald, M. (2018). Acoustic Emission Prediction of Supersonic Cold Flow Jets Using a CFD-CAA Hybrid Method. In Proc. Space Propulsion Conference, Seville, Spain.

6. Tam, C. K. W., Seiner, J. M., and Yu, J. C. (1986). Proposed relationship between broadband shock associated noise and screech tones. *Journal of Sound and Vibration* 1102, pp. 309–321.

7. Escartí-Guillem, M. S., Garcia-Raffi, L. M., and Hoyas, S. (2024). Review of launcher lift-off noise prediction and mitigation. *Results in Engineering* 23, pp. 1–21.

8. Zaman, K. B. M. Q. and Dahl, M. D. (1999). Aeroacoustic Resonance with Convergent–Divergent Nozzles. In Proc. 37th AIAA Aerospace Sciences Meeting and Exhibit, American Institute of Aeronautics and Astronautics, Reno, USA.

9. Zaman, K. B. M. Q., Dahl, M. D., and Bencic, T. J. (2001). Experimental Investigation of "Transonic Resonance" with Convergent–Divergent Nozzles. In Proc. 39th AIAA Aerospace Sciences Meeting and Exhibit, American Institute of Aeronautics and Astronautics, Reno, USA.

10. Génin, C. and Stark, R. (2016). Experimental investigation of cold flow TIC nozzles, a spectral analysis. In Proc. 52nd AIAA/SAE/ASEE Joint Propulsion Conference, American Institute of Aeronautics and Astronautics, Salt Lake City, USA.

11. Stark, R., Schneider, D., Martin, J., and General, S. (2019). Experimental Study on Jet Acoustics of Subscale Rocket Nozzles with a Different Divergent Contour Design. In Proc. 8th European Conference for Aeronautics and Space Sciences, Madrid, Spain.

12. Costa Ruiz, E., Stark, R., General, S., and Oschwald, M. (2019). Prediction of Subscale Rocket Engine Acoustic Emissions using CAA Hybrid Methods. In Proc. 8th European Conference for Aeronautics and Space Sciences, Madrid, Spain.

13. Stark, R., Wick, C., General, S., Möller, C., Aichner, T., Köglmeier, S., and Frey, M. (2023). Experimental Study of the Acoustical Interaction of a Subscale Rocket Nozzle Exhaust Jet and different Guide Tubes. *International Journal of Energetic Materials and Chemical Propulsion (IJEMCP)* 224, pp. 43–57.

14. Wilson, T. A., Beavers, G. S., DeCoster, M. A., Holger, D. K., and Regenfuss, M. D. (1971). Experiments on the Fluid Mechanics of Whisteling. *The Journal of the Acoustical Society of America* 501, pp. 366–372.

15. General, S. (2017). Background Oriented Schlieren: Hard- und Software für den mobilen Einsatz. *DIVA13, Lampoldshausen*,

16. Horn, B. K. P. and Schunck, B. G. (1981). Determing Optical Flow. *Artificial Intelligence* 171-3, pp. 185–203.

17. Stark, R. and Wagner, B. (2007). Mach Disk Shape in Truncated Ideal Contour Nozzles. In Proc. 26th International Symposium on Shock Waves, Göttingen, Germany.

18. Stark, R., Kronmüller, H., Zerjeski, D., and Wagner, B. (2003). Advanced Flow Visualisation Techniques in Cold Gas Subscale Nozzles, a Comparison. In Proc. 39th AIAA/ASME/SAE/ASEE, Joint Propulsion Conference & Exhibit, Huntsville, USA.

19. Frey, M., Makowka, K., Aichner, T., Stark, R., and Génin, C. (2017). The TICTOP nozzle — first experimental results. In Proc. EUCASS, 7th European Conference for Aerospace Sciences, Milan, Italy.

20. Stark, R. and Génin, C. (2019). Experimental Study of TICTOP Nozzles. In Proc. 31st International Symposium on Shock Waves, Nagoya, Japan.

21. Rieping, C., "Beitrag zum Einfluss von Ableitrohren auf die Strömungsablösung in Raketendüsen", BA thesis, Aachen, Germany: FH Aachen University of Applied Science, 2023.

22. Stark, R., Rieping, C., Aichner, T., and Frey, M. (2024). Experimental Study on the Effect of Chevrons on Flow Separation in Rocket Nozzles. In Proc. Proceedings of the Space Propulsion Conference, Glasgow, Scotland.

23. Stark, R., “Beitrag zum Verständnis der Strömungsablösung in Raketendüsen”, PhD thesis, Aachen, Germany: RWTH Aachen University, 2010.

24. Rieping, C., “Experimentelle Untersuchung der Pfeiftonentstehung im engsten Querschnitt von Raketendüsen”, MA thesis, Aachen, Germany: FH Aachen University of Applied Science, 2026.

7. APPENDIX

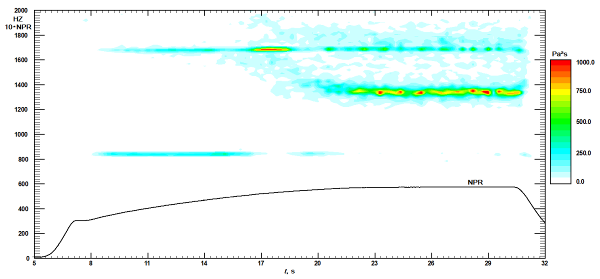

Figure 22: TICTOP B1 spectral density of the free jet configuration (PSD spectrogram). Taken from [13].